



**HAL**  
open science

## Revisiting of the physico-chemical properties of polyelectrolyte multilayers for a fine tuning of the immobilization of bacteria or nanoparticles

Ibtissem Gammoudi, Marion Mathélié-Guinlet, Zeineb Benabdallah, Fabien Moroté, Housseem Kahli, Laure Beven, R. Kalfat, A. Othmane, Marie-Hélène Delville, C. Grauby-Heywang, et al.

### ► To cite this version:

Ibtissem Gammoudi, Marion Mathélié-Guinlet, Zeineb Benabdallah, Fabien Moroté, Housseem Kahli, et al.. Revisiting of the physico-chemical properties of polyelectrolyte multilayers for a fine tuning of the immobilization of bacteria or nanoparticles. *Thin Solid Films*, 2020, 713, pp.138345. 10.1016/j.tsf.2020.138345 . hal-02941584

**HAL Id: hal-02941584**

**<https://hal.science/hal-02941584>**

Submitted on 17 Sep 2020

**HAL** is a multi-disciplinary open access archive for the deposit and dissemination of scientific research documents, whether they are published or not. The documents may come from teaching and research institutions in France or abroad, or from public or private research centers.

L'archive ouverte pluridisciplinaire **HAL**, est destinée au dépôt et à la diffusion de documents scientifiques de niveau recherche, publiés ou non, émanant des établissements d'enseignement et de recherche français ou étrangers, des laboratoires publics ou privés.

# **Revisiting of the physico-chemical properties of PAH/PSS polyelectrolyte multilayers for a fine tuning of the immobilization of bacteria or nanoparticles**

Ibtissen Gammoudi<sup>1,2,§</sup>, Marion Mathelié-Guinlet<sup>1,3,§</sup>, Zenieb Benabdallah<sup>1</sup>, Fabien Moroté<sup>1</sup>, Housseem Kahli<sup>1</sup>, Laure Beven<sup>4</sup>, Rafik Kalfat<sup>5</sup>, Ali Othmane<sup>6</sup>, M.H. Delville<sup>3</sup>,  
Christine Grauby-Heywang<sup>1\*</sup>, Corinne Dejous<sup>2</sup>, Touria Cohen-Bouhacina<sup>1</sup>

<sup>1</sup> Univ. Bordeaux, LOMA, CNRS UMR 5798, F-33400 Talence, France

<sup>2</sup> Univ. Bordeaux, IMS, CNRS UMR 5218, Bordeaux INP / ENSEIRB-MATMECA, F-33400 Talence, France

<sup>3</sup> CNRS, Univ. Bordeaux, Bordeaux INP, ICMCB, UMR 5026, 87 avenue du Dr Albert Schweitzer, 33608 Pessac, France

<sup>4</sup> Univ. Bordeaux, INRA, UMR 1332 Biologie du Fruit et Pathologie, 33882 Villenave-d'Ornon, France

<sup>5</sup> Institut National de Recherche et d'Analyse Physico-chimique, LMTA, LR15INRA003, T-2020 Sidi-Thabet, Tunisia

<sup>6</sup> Université de Monastir, Laboratoire de Biophysique, Faculté de Médecine, T-5019 Monastir, Tunisia

\*Corresponding author:

Christine Grauby-Heywang

Laboratoire Ondes et Matière d'Aquitaine (LOMA)

351 cours de la libération

33405 Talence Cedex, France

Phone number: 00 33 5 40 00 89 97

[christine.grauby-heywang@u-bordeaux.fr](mailto:christine.grauby-heywang@u-bordeaux.fr)

§ These authors contributed equally to this work.

## **Abstract**

Increasingly used in industrial coatings, polyelectrolytes multilayers (PEMs) are self-assembled systems made of the alternate deposition of oppositely charged polymers on substrates, usually built by the traditional layer-by-layer (LbL) method. Their properties strongly depend on environmental physico-chemical parameters. Due to the variety of conditions used in the literature on the one hand and the diversity of polyelectrolytes (PEs) systems on the other hand, it remains difficult to bring out general principles, leading now to a lack of a real understanding of the PEM buildup, from the macro- to the nanoscale. Here, combining for the first time acoustic and electrochemical methods with atomic force microscopy (AFM), in a systematic approach, we uncover the critical role of the deposition protocol in the growth regime of PEMs made of cationic poly (allylamine hydrochloride) (PAH) and anionic poly(4-styrene sulfonate, sodium) (PSS). Traditional dipping leads to thick, heterogeneous and relatively isolating PEMs whereas a spin-coating assisted method leads to thinner, homogeneous and more permeable PEMs. We also highlight that the pH and the ionic strength influence not only the electrostatic interactions and polyelectrolyte conformation in solution but also their organization after their adsorption on the substrate. Finally, our easily and rapidly adaptable protocol paves the way for promising potential bio-applications, since PEMs are successfully applied to the bacterial immobilization on substrates or as a coating for nanostructured biosensor transducer.

## **Key words**

Polyelectrolytes, Layer-by-Layer, Love Wave sensor, Atomic Force Microscopy AFM, Quartz Crystal microbalance with dissipation QCM-D, Cyclic Voltammetry

## 1. Introduction

The design of soft assemblies, with controlled properties at the nanoscale, has emerged as a challenging research area over the past decades, due to their implication in various coating applications, in optical devices [1], lubrication cosmetics [2], environment [3], energy [4] and medicine [5]. Different techniques have been developed for the self-assembly of materials with tunable properties (composition, structure, dimensions) to reach the requirements of the aforementioned fields. Among them, the Layer-by-Layer (LbL) technique, first introduced by Decher *et al.*, consists in the alternate deposition of oppositely charged molecules from aqueous solutions on a solid substrate, mostly through electrostatic interactions [6,7]. By definition, this method allows to tailor the physico-chemical properties of the final assembly by adjusting the intrinsic characteristics of the building blocks. Consequently, numerous studies have been devoted to the understanding of the buildup of these multilayers and of the involved key parameters, as well as to their possible applications [8–10]. In particular, the LbL technique has been initially and then widely applied to polyelectrolytes (PEs), poly(allylamine hydrochloride) (PAH) and poly(sodium 4-styrenesulfonate) (PSS) being probably the most studied polycation and polyanion, respectively, in this context.

Though the charge overcompensation among these charged polymers is known to control the formation process [11], it is still unclear how diverse physico-chemical parameters affect such a buildup. Originally, these stratified films appeared to grow linearly in thickness and mass with the number of deposited layer pairs, which can intertwine each other, leading to a robust structure [12–15]. However, a super linear (or exponential) growth regime was then suggested as another buildup mechanism: depending on the initial conditions and PEs properties, the film thickness increased more rapidly than previously thought, *i.e.* it was not any more proportional to the number of adsorbed layers

[16–18]. These two regimes, linear and exponential, were associated with the ability of the PEs to build up as either linear chains or aggregated complexes, diffusing in and out of the PE multilayer (PEM) core [19] and forming either a smooth film or a rough and heterogeneous one [20,21]. Physico-chemical properties such as environmental temperature [22], pH [23] and ionic strength [24,25] as well as the chemical nature of PE [20] influence the growth regime of such multilayers. In addition, to overcome the time consuming protocol of traditional LbL, different experimental methods have been proposed, adding new physical parameters playing a potential role in the buildup process. Thus a spin-coating assisted LbL method has been developed, that also comes along with a better control of PEM properties [26–28]. Similarly to dipping processes, physical parameters such as the PE molecular weight, the salt concentration, and the spin rate can modify the PEM architecture [29,30]. Dipping in stirred solutions [31] and ultrasonic-assisted LbL assembly [32] were also tested, along with assembly under a high gravity field [33] (substrate being in rotation as in spin-coating with PE solutions sprayed as tiny drops).

Unravelling the role of each of these parameters in the PEM buildup is essential to guarantee a control on the properties of the built nanocomposite films. This point is crucial to ensure subsequently their potential in various applications such as those developed in biotechnologies, especially in biosensor applications. Indeed, combined with specific nanoparticles or molecules (for instance proteins) and appropriately tuned, PEMs have already proven to be efficient and successful in the built-up of cytophilic or cytophobic surfaces [34–37], the immobilization of cells [38,39] or on the contrary in the inhibition of bio-adhesion [40–44] and even in enhancing immunodetection [45,46]. Though theoretical and experimental data mentioned so far tackle the influence of relevant physico-chemical properties, research focuses often on one parameter at a time,

leading to hazardous comparison as PEs and experimental conditions differ from one study to another.

In this context, we investigated here, in a systematic approach, the properties of these PEMS, depending on (i) the pH of the deposition solution and its ionic strength, and (ii) their deposition method (immersion versus spin-coating). Our goal was to define precisely the experimental conditions enabling to obtain PEMS with tunable properties paving the way for application opportunities. Indeed, we finally analyzed the efficiency of such PEMS (i) for the immobilization of bacteria, a pre-requirement for their characterization in physiological media, and (ii) as a coating for biosensor transducers involving nanoparticles. To fully characterize such PEMS and their potential in bio-applications, we combine two acoustic methods, (Love wave sensor [47] and Quartz Crystal Microbalance (QCM) [48]), with Atomic Force Microscopy (AFM) experiments on the one hand and electrochemical analysis on the other hand. To our knowledge, this work is the first to show that Love wave sensor method, an original technique usually developed for biosensor applications [49], is also well-suited to study PEM buildup.

## **2. Materials and methods**

### **2.1. Chemical and biological materials**

Two types of PE, purchased from Sigma-Aldrich (France), were used: cationic poly(allylamine hydrochloride) or PAH with a molecular weight of 56 kDa, and anionic poly(sodium 4-styrenesulfonate) or PSS with a molecular weight of 70 kDa. Tris Buffered Saline (TBS, 0.05 M Tris, 0.138 M NaCl, pH 7.4), and  $K_4[Fe(CN)_6]$  used for electrochemical measurements were also purchased from Sigma-Aldrich (France). Ultrapure water (Millipore, resistivity higher than 18 M $\Omega$ .cm, pH 5.5) was used as a solvent of the PEs, for

the rinsing steps and for the preparation of TBS. When necessary, the pH of PE's solutions was adjusted to the required value by adding HCl or NaOH (1 M).

Mica, purchased from Electron Microscopy Sciences (USA), was used for AFM characterizations, when they were not directly performed on the different sensors (Love wave, QCM-D, electrochemical ones). The potentiostat and screen printed electrodes for electrochemical experiments were purchased from Metrohm (Switzerland). Quartz crystals, coated with a gold layer, were purchased from Lot Quantum Design Sarl (France). Love wave devices were designed in the IMS Laboratory and produced in LAAS (UMR CNRS 8001, Toulouse, France). Gram negative *Escherichia coli* bacteria (MRE 162 strain) were a kind gift from the Centre d'Etudes du Bouchet, DGA (Direction Générale de l'Armement, France). Bacteria were grown on a solid Luria medium and incubated for 16 h at 37 °C. After scraping, bacteria were suspended in ultrapure water, their concentration being adjusted to  $10^8$  cells/mL.

Negatively and positively charged silica nanoparticles (SiO<sub>2</sub>-NPs) were home-made, following the procedure developed by Hartlen *et al.* [50] and detailed in our previous work [51].

## **2.2. Methods**

### **2.2.1. Layer-by-Layer (LbL) self-assembly methods**

The LbL method consists in a sequential and alternate deposition of the chosen polycation (PAH) and polyanion (PSS) on a solid substrate. The surface of mica, SiO<sub>2</sub> and gold substrates being negatively charged, the nature of the first layer was systematically PAH. Between each layer deposition, substrates were rinsed with ultrapure water, except in the case of Love wave sensor experiments where no rinsing step was necessary (as similar results were obtained with and without this step). These adsorption and rinsing steps

were repeated until reaching the desired number of layers. The final PEMs are denoted thereafter [PAH-(PSS-PAH)<sub>n</sub>], n being the number of bilayers. The nature of the last layer was also adapted to the targeted application, as shown later on.

Two techniques of deposition were used for this work: by immersion of the substrate into the solutions of PE or by spin coating, referred as I-LbL and SC-LbL methods, respectively.

For the I-LbL method, PAH and PSS solutions (10  $\mu$ L, 5 mg/mL in pure water) were simply deposited on the substrates for 10 min before rinsing with pure water, for QCM-D, AFM and CV experiments. In the case of Love wave experiments, PE solutions (0.5 mg/mL in TBS) were injected alternatively through a microfluidic system supplying an analysis chamber for 10-20 min at a flow rate equal to 20  $\mu$ L/min, with breaks for static conditions during PE layers deposition (thus providing conditions similar to those of immersion). In the case of QCM-D experiments, measurements were also performed in static conditions, PE solutions being injected in the analysis chamber through a millifluidic system at a flow rate of 1 mL/min.

For the SC-LbL method, substrates were placed in a spin-coating setup (Suss MicroTec) and PE solutions (10  $\mu$ L, 5 mg/mL in pure water) were deposited onto the surface before spinning at different rotation speeds (100, 500, 2000 rpm) and times (45, 120, 300 s) and rinsing with pure water (by 4 gentle deposition/aspiration cycles). At the end of the whole deposition process, substrates were left to dry for a few minutes. Under our experimental range, the spinning time did not significantly influence the PEMs roughness as shown by AFM, and was thus kept to its lowest value, 45 s, for a faster buildup. In addition, the roughness increased with the spinning speed and a speed of 100 rpm led to the minimal roughness when increasing the number of layers (data not shown).

### 2.2.2. Love wave sensor experiments

The real-time Love wave sensor was described previously in details [3,52–55]. Briefly it is made of a piezoelectric quartz substrate (AT cut), with interdigital transducers deposited by lift-off photolithography in order to generate pure shear horizontal acoustic waves propagating perpendicularly along the X crystallographic axis. A 4  $\mu\text{m}$   $\text{SiO}_2$  guiding layer, deposited on the substrate through plasma-enhanced chemical vapor deposition, confines the acoustic wave energy near the surface to maximize the sensor sensitivity [53], resulting in the so-called Love wave. Once placed in the retroaction loop of a radio-frequency amplifier, the synchronous frequency of the bare sensor is close to 117 MHz in agreement with the value previously reported [53]. Any modification of mass or viscoelastic properties at the sensor surface is electronically measured through a frequency shift ( $\Delta f_{\text{Love}}$ ). At last, the analysis chamber of the setup is supplied thanks to a programmable syringe pump (BS8000, Bioseb, France) through a microfluidic network. This device insures a homogenous and controlled flow on the sensitive path of the propagating acoustic wave [3,52,54]. In the case of PEs, the time of deposition was optimized in previous works [3,52], and fixed at 10 min, this time being sufficient to adsorb each PE (0.5 mg/mL in TBS) on the  $\text{SiO}_2$  sensor surface.

### 2.2.3. Quartz crystal microbalance with dissipation (QCM-D) experiments

QCM-D was used to study in real-time the changes induced by the PE deposition on the resonance of a quartz crystal (the resonance frequency of the bare device being 5 MHz), by following the frequency shift ( $\Delta f_{\text{QCM}}$ ), linked to the changes in adsorbed mass  $\Delta m$  through the Sauerbrey equation:  $\Delta m = -\frac{\rho_q t_q \Delta f_n}{n f_0}$ , where  $\rho_q$  is the specific density of the quartz crystal (2.648  $\text{g}\cdot\text{cm}^{-3}$ ),  $t_q$  its thickness (30 nm),  $f_0$  its fundamental frequency in air (4.95 MHz) and  $\Delta f_n$  is the change of resonance frequency at the first overtone ( $n = 1$ ) [56].

The experimental setup was made of a quartz crystal carrying a gold electrode enclosed in an analysis chamber connected to a millifluidic system for injection of solutions. Before each experiment, quartz substrates were sonicated in an ultrapure water bath containing dishwashing liquid for 15 minutes at a temperature of 60°C. After cleaning, substrates were equilibrated by injecting ultrapure water in the analysis chamber for at least 30 min., until observing a constant baseline of frequency shift  $\Delta f$ . Adsorption-rinsing cycles were then repeated by successive injections to build the PEM on the crystal in static conditions, 1 mL of each PE solution (5 mg/mL in water) being injected in the chamber and incubated for 15 min. Stabilization and experiments were made at room temperature.

#### **2.2.4. AFM experiments**

AFM experiments were carried out with a Bioscope II operating with the NanoScope V controller (Bruker, France), PEMs being deposited on mica or SiO<sub>2</sub> substrates. All AFM morphological characterizations were performed in tapping mode, in its repulsive dominant regime, for which the contrast of images is predominantly topographic. To this end, data were recorded with commercial cantilevers with a spring constant of about 40 N/m and a corresponding measured resonance frequency around 190 kHz, at a scan rate of 0.5–1.0 Hz. For thickness measurements, the contact mode was on the contrary privileged: AFM tip, with a spring constant of 0.12 N/m, was used as a rake to completely remove the material from its substrate on a defined area and so as to determine the layer thickness from height profiles. Different areas were systematically imaged, using independent samples, to ensure the repeatability and reproducibility of the results.

#### **2.2.5. Cyclic voltammetry measurements**

Cyclic voltammetry (CV) is an electrochemical method consisting in the application of a cyclic variable potential of a working electrode in order to measure corresponding

oxidation and reduction currents of the species contained in the studied medium. As such, it can also be used to detect and quantify any alteration due to the presence of heterogeneous material adsorbed on the electrode surface. Resulting CV curves show the presence of peaks characterized by a current intensity (mentioned later as  $I_a$  and  $I_c$  for oxidation and reduction, respectively) and a potential value ( $E_a$  and  $E_c$ ). In particular, the peak-to-peak separation ( $E_a - E_c$ ) gives access to the electrochemical reversibility of the electron transfer at the working electrode. In addition, the Randles-Sevcik equation enables to calculate the diffusion coefficients of our redox species in the contact of electrodes (nude or functionalized) [57]. This equation is  $i_{a/c} =$

$$0.446nFAC_{a/c} \left( \frac{nFvD_{a/c}}{RT} \right)^{1/2}, \text{ where:}$$

- $i_{a/c}$  is the current peak (A);
- $v$  is the scan speed ( $V \cdot s^{-1}$ );
- $n$  is the number of electrons transferred in the redox event;
- $F$  is the Faraday constant;
- $A$  is the surface of the electrode ( $cm^2$ );
- $C_{a/c}$  is the corresponding concentration ( $mol \cdot cm^{-3}$ );
- $D_{a/c}$  is the corresponding diffusion coefficient ( $cm^2 \cdot s^{-1}$ );
- $R$  is the ideal gaz constant;
- $T$  is the temperature (K).

Voltammetry measurements were carried out using a Metrohm 910 PSTAT mini potentiostat and a commercial and disposable system made of three screen-printed electrodes, a gold working electrode, a carbon auxiliary one and an Ag/AgCl reference one (reference 6.1208.210, Metrohm, France). Experiments were performed at room temperature using a 10 mM solution of  $K_4Fe(CN)_6 \cdot 3H_2O$  in TBS, within a potential range from -0.40 V to +0.60 V, adapted to the concerned  $Fe^{2+}/Fe^{3+}$  redox couple, at a scan rate of  $100 \text{ mV} \cdot s^{-1}$ , starting from the potential value at -0.40 V.

### 3. Results and discussion

#### 3.1. Investigation of the physical parameters affecting the PEM buildup

In the following part, the effect of pH and ionic strength and the influence of the deposition method of PEs (I-LbL versus SC-LbL) on the PEM buildup is investigated by Love wave sensor experiments and more conventional techniques (QCM-D, AFM and CV).

##### 3.1.1. Influence of pH

PEs being intrinsically highly charged, the pH is expected to play an important role in the PEM buildup. Under 'conventional' pH ranges, PSS ( $pK_a = 1$  [58]) is always highly negatively charged and its charge density is not significantly affected by varying the pH. On the contrary, considering the  $pK_a$  of PAH estimated at 8.5 [59], varying the pH can strongly affect the overall PE charge. We thus studied by Love wave sensor, under static conditions, the deposition of [PAH-(PSS-PAH) $_n$ ] PEMs at two pH values of the PAH solution, namely below ( $pH 7.2$ ) and above ( $pH 9.0$ ) its  $pK_a$  while the pH of the PSS solution was fixed at 7.2.

Figure 1a shows the real-time  $\Delta F_{Love}$  frequency shifts from the reference (bare sensor) after each PE injection, at the two pH values of the PAH solution. Typical "stairs" patterns are observed: each injection induces an increase of  $\Delta F_{Love}$  (in absolute value) and a stabilization after a few minutes, as expected in the case of a regular PE deposition process. However the  $\Delta F_{Love}$  amplitude depends on the pH of the PAH solution. At  $pH 7.2$  (black curve in Figure 1a), the deposition of each PAH layer induces a shift from 5 to 20 kHz, increasing with the number of previously deposited layers. At  $pH 9.0$  (red curve in Figure 1a), the absolute values of  $\Delta F_{Love}$  are clearly lower and do not increase as drastically with the number of previous layers. Finally, after the deposition of a [PAH-

[PSS-PAH]<sub>1.5</sub>] PEM, the cumulative frequency shift is significantly increased by 40 kHz when the PAH solution is at pH 7.2. A  $\Delta F_{\text{Love}}$  frequency shift being related to a modification of mass or viscoelastic properties at the sensor surface, these results show a more efficient adsorption of PEs at pH 7.2 than at pH 9.0.

As previously mentioned, PSS is always highly negatively charged under our experimental conditions. Given the pKa of PAH, the rate of protonated PAH monomers is estimated at 95% at a pH = 7.2, while decreasing at 24% at a pH = 9.0. This difference explains why the electrostatic interactions with the negatively charged SiO<sub>2</sub> surface or PSS layers are favored at this lower pH 7.2, leading to higher  $\Delta F_{\text{Love}}$  values. In addition, the deposition of PSS layers (at least until the buildup of a [PAH-(PSS-PAH)<sub>2</sub>] PEM) is also affected by the charge density of PAH, since the corresponding  $\Delta F_{\text{Love}}$  frequency shifts are significantly higher when the PAH solution pH is equal to 7.2. These observations are in agreement with previous reports [60,61] mentioning that PEMs should be neutral at the macroscopic level.

The influence of the pH on the topography of the surface resulting from the deposition of [PAH-(PSS-PAH)<sub>3</sub>] PEMs was further investigated by AFM (Figure 1b). Films are characterized by more or less irregular structures/aggregates and an increased roughness as compared to the bare SiO<sub>2</sub> surface (initial roughness of 3.2 nm): 18 nm and 41 nm in the case of PEMs made with a PAH solution at pH 7.2 and 9.0, respectively. If pH is set at 7.2 (pH < pKa), PEMs are also more homogenous probably resulting from a more homogenous deposition process due to high electrostatic interactions. If pH is set at 9 (pH > pKa), because of the decrease of the inter and intra-chain electrostatic interactions, a more globular chain conformation of PAH is expected [62], associated to a more heterogeneous and rougher surface of PEM observed by AFM.

### 3.1.2. Influence of the ionic strength

In addition to the effect of the pH, the presence of salt in the PE solutions is expected to strongly modify the architecture of the PEM, since the ionic strength also dictates the strength of the inter- and intra-chain interactions, and their possible rearrangements and detachments. Consequently, hereafter, we investigated the effect of an increased concentration of NaCl (from the intrinsic NaCl concentration in TBS, 0.138 M, to 1.500 M) in both PAH and PSS solutions (Figure 2a). The lowest tested NaCl concentration leads to the typical expected stair-step pattern, showing the actual sequential deposition of PE, as shown previously. At the highest concentration (1.50 M, Figure 2a), the  $\Delta F_{\text{Love}}$  frequency shifts are higher than in the native buffer solution suggesting a thicker PEM, in agreement with previous studies [62]·[63]. However signals are irregular and poorly reproducible. The plateaus corresponding to a steady state after deposition of either PAH or PSS are often missing, an increase of  $\Delta F_{\text{Love}}$  being even systematically observed in the case of PSS layers. These results suggest that, under such conditions, PEs do not adsorb efficiently on the surface or are even released from it. This can be explained by the conformational changes of PEs induced by the ionic strength. Indeed, at high ionic strength PEs are deposited in a globular conformation whereas at low ionic strength they tend to form rod-like chains [64], as schematized in Figure 2b.

This change in the chain conformation is due to the charge screening effect generated by the salts, with a concomitant decrease of the interaction between PEs of opposite charge [64]. It has been also reported that salts could act as “lubricants” of the motion of PE molecules interacting with oppositely charged surfaces [65]. A possible competition between ions and PEs has also been suggested [66]. When increasing salt concentration, all these proposed mechanisms are expected to lead to thicker but also more fragile films. The possible detachment of the PEs from the surface and a reduced probability of chain

interpenetration could explain the irregular shape of the  $\Delta F_{\text{Love}}$ -versus time curves observed at 1.5 M NaCl in the present work.

Overall, Love wave experiments finally show that [PAH-(PASS-PAH)<sub>n</sub>] buildup is much more efficient with the intrinsic NaCl concentration of TBS (0.138 M) and at neutral pH.

### 3.1.3. Influence of the deposition method

Investigating PEM buildup mechanism, we then wondered if the deposition method would influence its properties, especially in terms of thickness and roughness that are critical parameters for potential biotechnological purposes. Hereafter, we investigate the merits of the I-LbL (immersion) and SC-LbL (spin coating) deposition methods with AFM, QCM-D and CV experiments. For the convenience of AFM characterization, PEs were dissolved in ultrapure water and PEMs were built on a very smooth surface of mica (roughness of 0.5 nm), before being dried at room temperature. Optimal conditions described in Material and Methods were used for deposition by the SC-LbL method (100 rpm, 45 s).

*QCM-D measurements:* similarly to Love wave sensor experiments, the sequential deposition of [PAH-(PSS-PAH)<sub>n</sub>] PEMs is confirmed by an overall increase of the absolute value of the  $\Delta f_{\text{QCM}}$  frequency shift for both I-LbL and SC-LbL methods (Figure 3a), in QCM-D experiments. However, the lower values of  $\Delta f_{\text{QCM}}$  obtained by the SC-LbL method are significant of lower deposited masses, according to the Sauerbrey equation (see Materials & Methods). Masses are estimated at 3,200 ng/cm<sup>2</sup> and 1,100 ng/cm<sup>2</sup> for the I-LbL and SC-LbL methods, respectively, after the deposition of [PAH-(PSS-PAH)<sub>3</sub>] PEMs. Such masses are higher than other previously reported using QCM-D: for instance, around 1,100-1,300 ng/cm<sup>2</sup> in the case of PEMs made of 10 bilayers of PVA/PAA and PVA/PSS

[67], or around 475 ng/cm<sup>2</sup> in the case of PEMs made of 7 bilayers of PEI/PSS [68], prepared by I-LbL in both cases. Such differences are likely due to different experimental conditions (pH, concentration and nature of PEs ...). Furthermore, the two methods show a very different trend when increasing the number of layers. The steady-state frequency shift  $\Delta f_{\text{QCM}}$ , and thus the adsorbed mass, increases with the number of layers in the case of the I-LbL method. Nonetheless, the increasing shift induced by each (PSS-PAH) bilayer is not homogeneous along with the deposition process. When the SC-LbL method is used, the frequency shift after each bilayer is more constant (~20 kHz) but it encompasses oscillations being alternatively positive and negative (Figure 3a).

*AFM experiments:* To further understand this phenomenon, AFM imaging, in air, was performed on both systems (Figures 3b-e). Images show that PEMs, formed by SC-LbL or I-LbL methods, are made of aggregates distributed all over the mica surface (Figure 3b). Despite similar structures, it is clear that PEs aggregates formed by the I-LbL method are larger than those formed by the SC-LbL one. Scratching experiments (Figures 3c-d) at different steps of the deposition process of PEMs showed that, for both methods, the total thickness increases with the number of deposited layers, as expected, the I-LbL method leading to thicker films (whatever the number of layers, 3 or 7) than SC-LbL (Figure 3e). Mean thicknesses mentioned in this work with the I-LbL method are higher than those reported for instance at 3.5 nm in the similar case of [(PSS-PAH)<sub>5</sub>] PEMs (70 kDa both) deposited by immersion in water on a PEI-coated gold substrate[62]. On the contrary, the thicknesses obtained with the SC-LbL method are lower, but in the similar range, than values previously reported with a spin method at 1.65 nm per [PSS-PAH] PEM (70 kDa and 15 kDa, respectively) [69], or at 2.1-2.2 nm for a [PAH-PSS] PEM (both 70 kDa) [70]. In the case of the I-LbL technique, the increase of thickness is not strictly proportional to the number of layers: it increases roughly from 3 nm to 11 nm for 3 and 7 layers,

respectively. Such a hypothesis is in agreement with studies revealing an exponential growth regime for [(PAH-PSS)<sub>n</sub>] systems, where the thickness is not only a function of the PE conformation in the bulk but also of the specific properties of the surface-solution interface [63]. In particular an increasing roughness at each deposition step would increase the adsorption surface and thus the amount of adsorbed PE. Such an increase is observed by AFM, the roughness increasing from 4-5 nm to 9 nm with 3 and 7 deposited layers, respectively.

In the case of the SC-LbL method, QCM-D measurements confirm the overall deposition of PEMs by the global increase of the frequency shifts  $\Delta f_{\text{QCM}}$ . However, the oscillating behavior of this parameter also suggests that PEs could interpenetrate each other and reorganize into the film according to previously observed properties of adsorbed PEMs made of the alternate deposition of PSS and poly[2-(dimethylamino)ethyl methacrylate] PDEM [71]. In addition, the AFM measurements show that the thickness and the roughness of each deposited layer remain roughly constant during the SC-LbL deposition process (Figure 3e), and clearly lower than with the I-LbL method. All these results support the hypothesis of a PEM buildup likely following a linear growth regime by the SC-LbL method, with an interpenetration and a reorganization of PE chains, and leading to thinner and more homogeneous PEMs.

*CV measurements:* PEMs were then studied by CV, in order to test their permeability layer after layer and also their potential use in electrochemical biosensing devices. They were deposited sequentially onto a gold working electrode which was immersed in a TBS solution containing the Fe(CN)<sub>6</sub><sup>3-/4-</sup> couple.

Figure 4a shows typical CV curves obtained with a gold electrode, bare or covered with a [PAH-(PSS-PAH)<sub>n</sub>] PEM with n=3, formed either by the I-LbL or the SC-LbL methods. In

the absence of any layer at the electrode surface, oxidation and reduction peaks are observed due to the presence in the solution of the  $\text{Fe}(\text{CN})_6^{3-/4-}$  redox couple. In the case of the I-LbL method, the deposition of sequential [(PSS-PAH)] bilayers induces (i) a decrease of oxidation and reduction currents and (ii) a regular increase of  $\Delta E = (E_a - E_c)$ , both significant of the mass transfer to the electrode (Figures 4b-c). Similar results are observed when PEMs are built using the SC-LbL method (Figure 4).

In both cases (I-LbL and SC-LbL methods), the decrease of oxidation and reduction currents can be assigned to the increasing difficulty for the electroactive complex in solution to reach the electrode's surface after each deposition step. This was also shown by Elzbieciak *et al.* in the case of (PEI/PSS)<sub>n</sub> PEMs [72] and Harris and Bruening on (PAH/PSS)<sub>n</sub> and (PAH/PAA)<sub>n</sub> PEMs [73]. However, the differences observed in between the two deposition methods both in extent and trend as shown in Figure 4c, support the hypothesis of two different growth regimes.

Quantitatively, the diffusion coefficients of the redox species at the electrode ( $D_a$  and  $D_c$ ) were calculated based on the Randles-Sevcik equation:  $D_a$  was shown to decrease by 25 % vs. 57 % while  $D_c$  dropped by 46 % vs. 84 % after the deposition of three bilayers by SC-LbL and I-LbL respectively (Table 1), convincingly showing that PEMs are less permeable when prepared by the I-LbL method. Isolating efficiency of the coating is thus higher with the I-LbL method (at least after the first bilayer), PEMs made by SC-LbL deposition being more permeable to the electroactive molecules present in solution. However, our previous results suggest that PEMs by SC-LbL are more organized and homogeneous, implying that higher thickness of PEMs prepared by the I-LbL method might prevail on the more organized structure of PEMs made par the SC-LbL one.

Table 1. Diffusion coefficients of the redox species through the PEM built either from I-LbL and SC-LbL methods.

	<b>Diffusion coefficients (<math>10^{-6} \text{ cm}^2 \cdot \text{s}^{-1}</math>)</b>	
<b>I-LbL method</b>	Bare electrode	Electrode recovered by a [PAH-(PSS-PAH) <sub>3</sub> ] PEM
Oxidation current ( $i_a$ )	2.8	1.2
Reduction current ( $i_c$ )	2.5	0.4
<b>SC-LbL method</b>	Bare electrode	Electrode recovered by a [PAH-(PSS-PAH) <sub>3</sub> ] PEM
Oxidation current ( $i_a$ )	3.2	2.4
Reduction current ( $i_c$ )	2.8	1.5

Noteworthy is the fact that our diffusion coefficients are higher than those reported by Ghostine and Schlenoff [74] in the range of  $10^{-9} \text{ cm}^2/\text{s}$ , measured with the same redox couple on PEMs made of PDADMA and PSS. Nonetheless, the different nature of one PE and the number of deposited bilayers (10 bilayers in this study) could explain such a difference.

To conclude, though the (PAH-PSS) systems have been widely investigated in the literature, different protocols, with different numbers of layers and / or under different environmental conditions, have led to confusing, even sometimes contradictory, results. Here, by re-investigating this system at the nanoscale, by studying its properties with complementary techniques (Love waves, AFM, QCM-D and CV), in a systematic approach and under strict conditions free of “parameters interpretation”, we showed notably how the deposition process of PEs influences the intrinsic characteristics of the final PEM. I-LbL and SC-LbL methods lead to PEMs likely growing with two different growth regimes. The former process induces thicker, rougher and less permeable films than those obtained with the latter one. Overall, our results are in agreement with those of previous studies aiming also at developing methods to accelerate the PEM buildup, such as dipping the substrate in stirred solutions or applying a high gravity field. As in the case of the SC-

LbL technique, these methods lead to smoother and more homogenous films, as compared to conventional dipping.

### **3.2. PEMs, a way to sense or to attach diverse (bio)systems**

Depending on the deposition process, the physico-chemical characteristics of the PEM can thus be tuned. This is especially interesting when targeting biotechnological applications, which do not all require the same characteristics of the support. When the adhesion of cells requires rather soft and hydrated cushions isolating cells from the support, the functionalization of electrodes for biosensing needs on the contrary thinner, organized, more permeable (yet adhesive) films, for the further detection of bio-chemical systems in the nanometric range.

In this context, PEMs built from the I-LbL method and the SC-LbL one appear well adapted in the first and second domains of application, respectively. Brief illustrations in both domains are proposed in the following parts.

#### **3.2.1 Immobilization of bacteria on PEMs built by the I-LbL method**

Imaging cellular systems, under physiologically conditions, require their immobilization on substrates. Different methods have been developed for this purpose, including self-assembled monolayers or polymer brushes (poly-L-lysine and PEI), but the use of PEMs could also provide an interesting alternative method.

In this work, Gram negative *E. coli* bacteria were deposited onto either bare mica or mica functionalized with [PAH-(PSS-PAH)<sub>3</sub>] PEMs built using the I-LbL method, and imaged by AFM either under air ambient conditions or in ultrapure water (Figure 5). When deposited on bare mica and imaged in air, bacteria form more or less dense aggregates

which cover only a small fraction of the substrate. Imaged in liquid, all the bacteria are detached from the mica surface, and pushed away by the AFM tip. On the opposite, when deposited on the same mica surface covered with a PEM ending with a PAH layer and imaged in liquid over time, the bacteria population, this time, homogeneously covers the surface and remains attached to the PEM. This approach does provide a new alternative to study bacteria in their media. Similar results are obtained with Gram positive *B. subtilis* bacteria (data not shown).

Even if the organization of *E. coli* and *B. subtilis* envelopes is different, bacteria surfaces both exhibit a negative charge, which prevents their adhesion on such a negative substrate, as mica. In the presence of PEMs, ending with a positively charged PAH outermost layer, electrostatic interactions with *E. coli* external membrane or *B. subtilis* cell wall are favored and are strong enough to prevent the cell motion in liquid under the AFM tip. At the same time, under these conditions, the AFM images suggest the biocompatibility of this kind of substrate, though usually designed as anti-adhesion/bactericidal coatings [44], since bacteria keep their typical rod shape and dimensions, with no sign of cell wall collapse. These results are in good agreement with a previous study dealing with bacteria immobilized on PEMs of various surface charges, and highlighting the crucial role of electrostatic interactions for cell attachment [38].

### **3.2.2. Immobilization of NPs on PEMs built by the SC-LbL method: nanostructured films for sensor applications**

Another great promise of PEMs is their application in biosensors, which require an optimal control not only in terms of surface charge but also in terms of surface roughness. Hereafter, we present a possible application of PEMs built with the SC-LbL method for the

design of nanostructured surfaces based on the adsorption of SiO<sub>2</sub>-NPs on such PEMs. Negatively charged 200 nm diameter SiO<sub>2</sub>-NPs (NPs<sup>-</sup>) were thus deposited, at a concentration of 5 g/L, by spin coating (20 s, 200 rpm) onto a [PAH-(PSS-PAH)<sub>3</sub>] PEM. After a decrease in intensities due to the PEM buildup (as shown above), the electrochemical measurements (Figure 6a) shows a further decrease in CV signals. This proves the actual electrostatic interactions of the NPs on the PEM, that slows down the charge transfer of Fe(CN)<sub>6</sub><sup>3-/4-</sup> at the electrode.

Positively charged NPs (100 nm NPs<sup>+</sup>) were deposited under the same experimental conditions on a [PAH-(PSS-PAH)<sub>3</sub>-PSS] PEM. Surprisingly, the presence of NPs did not induce any significant modification of the quantity of redox species able to reach the electrode (Figure 6b), though the coating was confirmed by AFM (Figure 6c). This might be explained by the presence of the positively charged surface of the NPs, which interact even less than the PAH layer (Figure 6a) with the kinetics at the electrode surface [75].

Our results show that the coating of PEMs by silica NPs is driven by electrostatic interaction, and confirm other works in the literature [76,77].

A successful example of such a kind of application has been recently shown, with the design of a biosensor with a working electrode previously covered by positively charged silica NPs immobilized on a PEM and easily functionalized by antibodies for the specific detection of bacteria [78]. The presence of the NPs layer greatly enhanced the performances of the sensor, as also shown in other cases in terms of sensitivity and selectivity [79].

In conclusion of this last part, we showed that PEMs properties can be specifically tuned, depending on the experimental conditions used for their design and their outermost layer,

for the immobilization of various objects and in a biocompatible manner. We have thus found a common easily and rapidly adaptable protocol, based on the intrinsic architecture of the PEM, well beyond the current multiple different strategies applied for biomedical applications. Such a protocol is likely transferable to other biotechnological applications such as optics and cosmetics for which nanoscale controls and characterizations are critical. Nonetheless, the biologically-relevant applications of PEMs still need to be fully investigated, especially under physiological conditions (pH and temperature). Indeed, our results, obtained at room temperature and neutral pH, might be affected notably at physiological temperature: the cross-correlation of each, and every physical and environmental parameters that could affect the PEM, and in turn its applicability to technological applications, remain to be fully understood.

#### **4. Conclusion**

To conclude, we have combined four complementary methods, from the microscale down to the nanoscale, to fully characterize, optimize and understand in a systematic approach the build-up of PEMs made of PAH and PSS. This build-up was performed by two methods (immersion vs spin-coating) to study the functionalization of three types of surface (mica, silica and gold), leading to systems with tunable properties. To our knowledge, this is also the first time that the Love wave sensor method is applied to such a study. We highlighted the important role of PE charge density (through adapted pH and ionic strength of the solutions) in the growth regime of the PEM. Moreover, the deposition method, *i.e.* immersion vs. spin-coating, which has often been neglected even ignored so far in the literature, is in fact a critical parameter that researchers should take into account from now on. Its impact on the PEM subsequent properties is crucial, leading to either a thick isolating film or a thin permeable one. Finally, the two types of PEMs were applied in two

domains of bio-applications needing opposite prerequisites in terms of surface functionalization: the immobilization on the one hand of biological samples (bacteria) making possible their observation in biocompatible conditions, and on the other hand of inorganic materials with a size in the nanometric range (SiO<sub>2</sub>-NPs). These two different applications only require to adjust in a simple way the nature of the outermost layer and the method of deposition, paving the way of many other bio-applications.

## **Acknowledgements**

The authors thank the Région Aquitaine and CNRS (France) for supporting this work through the equipment of platform used in this work: NanoSpectroImagerie (NSI - CPER COLA2) and TAMIS (IMS). They are also grateful to H. Tabargue (IMS Bordeaux, CNRS UMR 5218) who designed PDMS chips in the frame of the ANR project BIOALERT (Agence Nationale de la Recherche, PRECODD program, ANR-06-ECOT-004), and to J.-L. Lachaud and I. Favre (IMS Bordeaux, CNRS UMR 5218) for the design of microfluidic devices. The authors thank M. Benoît (Réseau Technologique de Base, LAAS-CNRS, Toulouse, France) for realizing acoustic wave delay-lines, and D. Moynet (retired from the University of Bordeaux) for his expertise and participation in experiments with bacteria and Love wave devices.

## **Funding**

The authors are grateful to the Direction Générale de l'Armement (DGA, Ministère de la Défense, France), the Région Aquitaine (France) and LOMA for their financial support

through the Ph.D. grant of M. Mathelié-Guinlet, the CMCU grant of I. Gammoudi (bilateral PHC program France-Tunisia, project No. 10G1103).

## References

- [1] C.-H. Lin, H.-L. Cho, Y.-H. Yeh, M.-C. Yang, Improvement of the surface wettability of silicone hydrogel contact lenses via layer-by-layer self-assembly technique, *Colloids Surf. B Biointerfaces*. 136 (2015) 735–743. <https://doi.org/10.1016/j.colsurfb.2015.10.006>.
- [2] S. Lee, S. Zürcher, A. Dorcier, G.S. Luengo, N.D. Spencer, Adsorption and Lubricating Properties of Poly(l-lysine)-graft-poly(ethylene glycol) on Human-Hair Surfaces, *ACS Appl. Mater. Interfaces*. 1 (2009) 1938–1945. <https://doi.org/10.1021/am900337z>.
- [3] I. Gammoudi, V. Raimbault, H. Tarbague, F. Moroté, C. Grauby-Heywang, A. Othmane, R. Kalfat, D. Moynet, D. Rebière, C. Dejous, T. Cohen-Bouhacina, Enhanced bio-inspired microsensor based on microfluidic/bacteria/love wave hybrid structure for continuous control of heavy metals toxicity in liquid medium, *Sens. Actuators B Chem.* 198 (2014) 278–284. <https://doi.org/10.1016/j.snb.2014.01.104>.
- [4] Y. Xiang, S. Lu, S.P. Jiang, Layer-by-layer self-assembly in the development of electrochemical energy conversion and storage devices from fuel cells to supercapacitors, *Chem. Soc. Rev.* 41 (2012) 7291–7321. <https://doi.org/10.1039/C2CS35048C>.
- [5] W. Tong, X. Song, C. Gao, Layer-by-layer assembly of microcapsules and their biomedical applications, *Chem. Soc. Rev.* 41 (2012) 6103–6124. <https://doi.org/10.1039/C2CS35088B>.
- [6] G. Decher, J. Schmitt, Fine-Tuning of the film thickness of ultrathin multilayer films composed of consecutively alternating layers of anionic and cationic polyelectrolytes, in: C. Helm, M. Lösche, H. Möhwald (Eds.), *Trends Colloid Interface Sci. VI*, Steinkopff, 1992: pp. 160–164.
- [7] G. Decher, Fuzzy Nanoassemblies: Toward Layered Polymeric Multicomposites, *Science*. 277 (1997) 1232. <https://doi.org/10.1126/science.277.5330.1232>.
- [8] Hammond P. T., Form and Function in Multilayer Assembly: New Applications at the Nanoscale, *Adv. Mater.* 16 (2004) 1271–1293. <https://doi.org/10.1002/adma.200400760>.
- [9] X. Zhang, H. Chen, H. Zhang, Layer-by-layer assembly: from conventional to unconventional methods, *Chem. Commun.* 0 (2007) 1395–1405. <https://doi.org/10.1039/B615590A>.
- [10] S.T. Dubas, J.B. Schlenoff, Factors Controlling the Growth of Polyelectrolyte Multilayers, *Macromolecules*. 32 (1999) 8153–8160. <https://doi.org/10.1021/ma981927a>.
- [11] J.B. Schlenoff, H. Ly, M. Li, Charge and Mass Balance in Polyelectrolyte Multilayers, *J. Am. Chem. Soc.* 120 (1998) 7626–7634. <https://doi.org/10.1021/ja980350+>.
- [12] M. Lösche, J. Schmitt, G. Decher, W.G. Bouwman, K. Kjaer, Detailed Structure of Molecularly Thin Polyelectrolyte Multilayer Films on Solid Substrates as Revealed by Neutron Reflectometry, *Macromolecules*. 31 (1998) 8893–8906. <https://doi.org/10.1021/ma980910p>.
- [13] D. Yoo, S.S. Shiratori, M.F. Rubner, Controlling Bilayer Composition and Surface Wettability of Sequentially Adsorbed Multilayers of Weak Polyelectrolytes, *Macromolecules*. 31 (1998) 4309–4318. <https://doi.org/10.1021/ma9800360>.

- [14] F. Caruso, K. Niikura, D.N. Furlong, Y. Okahata, 1. Ultrathin Multilayer Polyelectrolyte Films on Gold: Construction and Thickness Determination, *Langmuir*. 13 (1997) 3422–3426. <https://doi.org/10.1021/la960821a>.
- [15] E. Guzmán, H.A. Ritacco, F. Ortega, R.G. Rubio, Growth of Polyelectrolyte Layers Formed by Poly(4-styrenesulfonate sodium salt) and Two Different Polycations: New Insights from Study of Adsorption Kinetics, *J. Phys. Chem. C*. 116 (2012) 15474–15483. <https://doi.org/10.1021/jp304522t>.
- [16] J. Ruths, F. Essler, G. Decher, H. Riegler, Polyelectrolytes I: Polyanion/Polycation Multilayers at the Air/Monolayer/Water Interface as Elements for Quantitative Polymer Adsorption Studies and Preparation of Hetero-superlattices on Solid Surfaces, *Langmuir*. 16 (2000) 8871–8878. <https://doi.org/10.1021/la000257a>.
- [17] D.L. Elbert, C.B. Herbert, J.A. Hubbell, Thin Polymer Layers Formed by Polyelectrolyte Multilayer Techniques on Biological Surfaces, *Langmuir*. 15 (1999) 5355–5362. <https://doi.org/10.1021/la9815749>.
- [18] C. Picart, P. Lavalle, P. Hubert, F.J.G. Cuisinier, G. Decher, P. Schaaf, J.-C. Voegel, Buildup Mechanism for Poly(L-lysine)/Hyaluronic Acid Films onto a Solid Surface, *Langmuir*. 17 (2001) 7414–7424. <https://doi.org/10.1021/la010848g>.
- [19] C. Picart, J. Mutterer, L. Richert, Y. Luo, G.D. Prestwich, P. Schaaf, J.-C. Voegel, P. Lavalle, Molecular basis for the explanation of the exponential growth of polyelectrolyte multilayers, *Proc. Natl. Acad. Sci.* 99 (2002) 12531–12535. <https://doi.org/10.1073/pnas.202486099>.
- [20] P. Lavalle, C. Gergely, F.J.G. Cuisinier, G. Decher, P. Schaaf, J.C. Voegel, C. Picart, Comparison of the Structure of Polyelectrolyte Multilayer Films Exhibiting a Linear and an Exponential Growth Regime: An in Situ Atomic Force Microscopy Study, *Macromolecules*. 35 (2002) 4458–4465. <https://doi.org/10.1021/ma0119833>.
- [21] R.A. McAloney, M. Sinyor, V. Dudnik, M.C. Goh, Atomic Force Microscopy Studies of Salt Effects on Polyelectrolyte Multilayer Film Morphology, *Langmuir*. 17 (2001) 6655–6663. <https://doi.org/10.1021/la010136q>.
- [22] M. Salomäki, I.A. Vinokurov, J. Kankare, Effect of Temperature on the Buildup of Polyelectrolyte Multilayers, *Langmuir*. 21 (2005) 11232–11240. <https://doi.org/10.1021/la051600k>.
- [23] S.S. Shiratori, M.F. Rubner, pH-Dependent Thickness Behavior of Sequentially Adsorbed Layers of Weak Polyelectrolytes, *Macromolecules*. 33 (2000) 4213–4219. <https://doi.org/10.1021/ma991645q>.
- [24] E. Guzmán, H. Ritacco, J.E.F. Rubio, R.G. Rubio, F. Ortega, Salt-induced changes in the growth of polyelectrolyte layers of poly(diallyl-dimethylammonium chloride) and poly(4-styrene sulfonate of sodium), *Soft Matter*. 5 (2009) 2130–2142. <https://doi.org/10.1039/B901193E>.
- [25] D.K. Kim, S.W. Han, C.H. Kim, J.D. Hong, K. Kim, Morphology of multilayers assembled by electrostatic attraction of oppositely charged model polyelectrolytes, *Thin Solid Films*. 350 (1999) 153–160. [https://doi.org/10.1016/S0040-6090\(99\)00351-X](https://doi.org/10.1016/S0040-6090(99)00351-X).
- [26] Y. Li, X. Wang, J. Sun, Layer-by-layer assembly for rapid fabrication of thick polymeric films, *Chem. Soc. Rev.* 41 (2012) 5998–6009. <https://doi.org/10.1039/C2CS35107B>.
- [27] F. Fadhilah, S.M. Javaid Zaidi, Z. Khan, M. Khaled, F. Rahman, P. Hammond, Development of multilayer polyelectrolyte thin-film membranes fabricated by spin assisted layer-by-layer assembly, *J. Appl. Polym. Sci.* 126 (2012) 1468–1474. <https://doi.org/10.1002/app.36879>.

- [28] Cho J., Char K., Hong J.-D., Lee K.-B., Fabrication of Highly Ordered Multilayer Films Using a Spin Self-Assembly Method, *Adv. Mater.* 13 (2001) 1076–1078. [https://doi.org/10.1002/1521-4095\(200107\)13:14<1076::AID-ADMA1076>3.0.CO;2-M](https://doi.org/10.1002/1521-4095(200107)13:14<1076::AID-ADMA1076>3.0.CO;2-M).
- [29] P.A. Patel, A.V. Dobrynin, P.T. Mather, Combined Effect of Spin Speed and Ionic Strength on Polyelectrolyte Spin Assembly, *Langmuir*. 23 (2007) 12589–12597. <https://doi.org/10.1021/la7020676>.
- [30] S.-S. Lee, K.-B. Lee, J.-D. Hong, Evidence for Spin Coating Electrostatic Self-Assembly of Polyelectrolytes, *Langmuir*. 19 (2003) 7592–7596. <https://doi.org/10.1021/la034263t>.
- [31] Y. Fu, S.-J. Li, J. Xu, M. Yang, J.-D. Zhang, Y.-H. Jiao, J.-C. Zhang, K. Zhang, Y.-G. Jia, Facile and Efficient Approach to Speed up Layer-by-Layer Assembly: Dipping in Agitated Solutions, *Langmuir*. 27 (2011) 672–677. <https://doi.org/10.1021/la104524k>.
- [32] C. Jiang, M. Cheng, H. Liu, L. Shao, X. Zeng, Y. Zhang, F. Shi, Fabricating Transparent Multilayers with UV and Near-IR Double-Blocking Properties through Layer-by-Layer Assembly, *Ind. Eng. Chem. Res.* 52 (2013) 13393–13400. <https://doi.org/10.1021/ie401769h>.
- [33] C. Jiang, X. Liu, C. Luo, Y. Zhang, L. Shao, F. Shi, Controlled exponential growth in layer-by-layer multilayers using high gravity fields, *J. Mater. Chem. A*. 2 (2014) 14048–14053. <https://doi.org/10.1039/C4TA02437K>.
- [34] J.D. Mendelsohn, S.Y. Yang, J. Hiller, A.I. Hochbaum, M.F. Rubner, Rational Design of Cytophilic and Cytophobic Polyelectrolyte Multilayer Thin Films, *Biomacromolecules*. 4 (2003) 96–106. <https://doi.org/10.1021/bm0256101>.
- [35] J. Chluba, J.-C. Voegel, G. Decher, P. Erbacher, P. Schaaf, J. Ogier, Peptide Hormone Covalently Bound to Polyelectrolytes and Embedded into Multilayer Architectures Conserving Full Biological Activity, *Biomacromolecules*. 2 (2001) 800–805. <https://doi.org/10.1021/bm015529i>.
- [36] T. Serizawa, M. Yamaguchi, T. Matsuyama, M. Akashi, Alternating Bioactivity of Polymeric Layer-by-Layer Assemblies: Anti- vs Procoagulation of Human Blood on Chitosan and Dextran Sulfate Layers, *Biomacromolecules*. 1 (2000) 306–309. <https://doi.org/10.1021/bm000006g>.
- [37] I. Gammoudi, M. Mathelie-guinlet, F. Morote, L. Beven, D. Moynet, C. Grauby-heywang, T. Cohen-bouhacina, Morphological and nanostructural surface changes in *Escherichia coli* over time, monitored by atomic force microscopy, *Colloids Surf. B Biointerfaces*. 141 (2016) 355–364. <https://doi.org/10.1016/j.colsurfb.2016.02.006>.
- [38] X. Zhu, S. Guo, T. He, S. Jiang, D. Jańczewski, G.J. Vancso, Engineered, Robust Polyelectrolyte Multilayers by Precise Control of Surface Potential for Designer Protein, Cell, and Bacteria Adsorption, *Langmuir*. 32 (2016) 1338–1346. <https://doi.org/10.1021/acs.langmuir.5b04118>.
- [39] N.E. Muzzio, M.A. Pasquale, D. Gregurec, E. Diamanti, M. Kosutic, O. Azzaroni, S.E. Moya, Polyelectrolytes Multilayers to Modulate Cell Adhesion: A Study of the Influence of Film Composition and Polyelectrolyte Interdigitation on the Adhesion of the A549 Cell Line, *Macromol. Biosci.* 16 (2016) 482–495. <https://doi.org/10.1002/mabi.201500275>.
- [40] T. Kruk, K. Szczepanowicz, D. Kręgiel, L. Szyk-Warszyńska, P. Warszyński, Nanostructured multilayer polyelectrolyte films with silver nanoparticles as antibacterial coatings, *Colloids Surf. B Biointerfaces*. 137 (2016) 158–166. <https://doi.org/10.1016/j.colsurfb.2015.06.016>.

- [41] B. Wang, T. Jin, Q. Xu, H. Liu, Z. Ye, H. Chen, Direct Loading and Tunable Release of Antibiotics from Polyelectrolyte Multilayers To Reduce Bacterial Adhesion and Biofilm Formation, *Bioconjug. Chem.* 27 (2016) 1305–1313. <https://doi.org/10.1021/acs.bioconjchem.6b00118>.
- [42] N.E. Muzzio, M.A. Pasquale, E. Diamanti, D. Gregurec, M.M. Moro, O. Azzaroni, S.E. Moya, Enhanced antiadhesive properties of chitosan/hyaluronic acid polyelectrolyte multilayers driven by thermal annealing: Low adherence for mammalian cells and selective decrease in adhesion for Gram-positive bacteria, *Mater. Sci. Eng. C.* 80 (2017) 677–687. <https://doi.org/10.1016/j.msec.2017.07.016>.
- [43] S. Guo, M.Y. Kwek, Z.Q. Toh, D. Pranantyo, E.-T. Kang, X.J. Loh, X. Zhu, D. Jańczewski, K.G. Neoh, Tailoring Polyelectrolyte Architecture To Promote Cell Growth and Inhibit Bacterial Adhesion, *ACS Appl. Mater. Interfaces.* 10 (2018) 7882–7891. <https://doi.org/10.1021/acsami.8b00666>.
- [44] L. Séon, P. Lavalley, P. Schaaf, F. Boulmedais, Polyelectrolyte Multilayers: A Versatile Tool for Preparing Antimicrobial Coatings, *Langmuir.* 31 (2015) 12856–12872. <https://doi.org/10.1021/acs.langmuir.5b02768>.
- [45] W. Yang, D. Trau, R. Renneberg, N.T. Yu, F. Caruso, Layer-by-Layer Construction of Novel Biofunctional Fluorescent Microparticles for Immunoassay Applications, *J. Colloid Interface Sci.* 234 (2001) 356–362. <https://doi.org/10.1006/jcis.2000.7325>.
- [46] F. Caruso, K. Niikura, D.N. Furlong, Y. Okahata, 2. Assembly of Alternating Polyelectrolyte and Protein Multilayer Films for Immunosensing, *Langmuir.* 13 (1997) 3427–3433. <https://doi.org/10.1021/la9608223>.
- [47] N. Moll, E. Pascal, D.H. Dinh, J.P. Pillot, B. Bennetau, D. Rebière, D. Moynet, Y. Mas, D. Mossalayi, J. Pistré, C. Déjous, A Love wave immunosensor for whole E. coli bacteria detection using an innovative two-step immobilisation approach., *Biosens. Bioelectron.* 22 (2007) 2145–2150. <https://doi.org/10.1016/j.bios.2006.09.032>.
- [48] K.A. Marx, Quartz Crystal Microbalance: A Useful Tool for Studying Thin Polymer Films and Complex Biomolecular Systems at the Solution–Surface Interface, *Biomacromolecules.* 4 (2003) 1099–1120. <https://doi.org/10.1021/bm020116i>.
- [49] Z. Xu, Y.J. Yuan, Implementation of guiding layers of surface acoustic wave devices: A review, *Biosens. Bioelectron.* 99 (2018) 500–512. <https://doi.org/10.1016/j.bios.2017.07.060>.
- [50] K.D. Hartlen, A.P.T. Athanasopoulos, V. Kitaev, Facile Preparation of Highly Monodisperse Small Silica Spheres (15 to >200 nm) Suitable for Colloidal Templating and Formation of Ordered Arrays, *Langmuir.* 24 (2008) 1714–1720. <https://doi.org/10.1021/la7025285>.
- [51] M. Mathelié-Guinlet, L. Béven, F. Moroté, D. Moynet, C. Grauby-Heywang, I. Gammoudi, M.-H. Delville, T. Cohen-Bouhacina, Probing the threshold of membrane damage and cytotoxicity effects induced by silica nanoparticles in Escherichia coli bacteria, *Adv. Colloid Interface Sci.* 245 (2017) 81–91. <https://doi.org/10.1016/j.cis.2017.04.012>.
- [52] I. Gammoudi, L. Blanc, F. Moroté, C. Grauby-Heywang, C. Boissière, R. Kalfat, D. Rebière, T. Cohen-Bouhacina, C. Déjous, High sensitive mesoporous TiO<sub>2</sub>-coated love wave device for heavy metal detection, *Biosens. Bioelectron.* 57 (2014) 162–170. <https://doi.org/10.1016/j.bios.2013.12.024>.
- [53] F. Razan, C. Zimmermann, D. Rebière, C. Déjous, J. Pistré, M. Destarac, B. Pavageau, Radio frequency thin film characterization with polymer-coated Love-wave sensor,

- Sens. Actuators B Chem. 108 (2005) 917–924. <https://doi.org/10.1016/j.snb.2004.12.093>.
- [54] H. Tarbague, J.-L. Lachaud, S. Destor, L. Velutini, J.-P. Pillot, B. Bennetau, D. Moynet, D. Rebière, J. Pistre, C. Dejous, PDMS (Polydimethylsiloxane) Microfluidic Chip Molding for Love Wave Biosensor, *ECS Trans.* 23 (2009) 319–325. <https://doi.org/10.1149/1.3183735>.
- [55] C. Zimmermann, D. Rebière, C. Déjous, J. Pistré, E. Chastaing, R. Planade, A love-wave gas sensor coated with functionalized polysiloxane for sensing organophosphorus compounds, *Sens. Actuators B Chem.* 76 (2001) 86–94. [https://doi.org/10.1016/S0925-4005\(01\)00578-0](https://doi.org/10.1016/S0925-4005(01)00578-0).
- [56] Y. Ebara, Y. Okahata, A Kinetic Study of Concanavalin A Binding to Glycolipid Monolayers by Using a Quartz-Crystal Microbalance, *J. Am. Chem. Soc.* 116 (1994) 11209–11212. <https://doi.org/10.1021/ja00104a001>.
- [57] N. Elgrishi, K.J. Rountree, B.D. McCarthy, E.S. Rountree, T.T. Eisenhart, J.L. Dempsey, A Practical Beginner’s Guide to Cyclic Voltammetry, *J. Chem. Educ.* 95 (2018) 197–206. <https://doi.org/10.1021/acs.jchemed.7b00361>.
- [58] O. Guillaume-Gentil, O.V. Semenov, A.H. Zisch, R. Zimmermann, J. Vörös, M. Ehrbar, pH-controlled recovery of placenta-derived mesenchymal stem cell sheets, *Biomaterials.* 32 (2011) 4376–4384. <https://doi.org/10.1016/j.biomaterials.2011.02.058>.
- [59] S.W. Cranford, C. Ortiz, M.J. Buehler, Mechanomutable properties of a PAA/PAH polyelectrolyte complex: rate dependence and ionization effects on tunable adhesion strength, *Soft Matter.* 6 (2010) 4175. <https://doi.org/10.1039/c0sm00095g>.
- [60] E. Guzmán, A. Mateos-Maroto, M. Ruano, F. Ortega, R.G. Rubio, Layer-by-Layer polyelectrolyte assemblies for encapsulation and release of active compounds, *Adv. Colloid Interface Sci.* 249 (2017) 290–307. <https://doi.org/10.1016/j.cis.2017.04.009>.
- [61] E. Guzmán, J.A. Cavallo, R. Chuliá-Jordán, C. Gómez, M.C. Strumia, F. Ortega, R.G. Rubio, pH-Induced Changes in the Fabrication of Multilayers of Poly(acrylic acid) and Chitosan: Fabrication, Properties, and Tests as a Drug Storage and Delivery System, *Langmuir.* 27 (2011) 6836–6845. <https://doi.org/10.1021/la200522r>.
- [62] E. Poptoshev, B. Schoeler, F. Caruso, Influence of Solvent Quality on the Growth of Polyelectrolyte Multilayers, *Langmuir.* 20 (2004) 829–834. <https://doi.org/10.1021/la035485u>.
- [63] J. Ruths, F. Essler, G. Decher, H. Riegler, Polyelectrolytes I: Polyanion/Polycation Multilayers at the Air/Monolayer/Water Interface as Elements for Quantitative Polymer Adsorption Studies and Preparation of Hetero-superlattices on Solid Surfaces †, *Langmuir.* 16 (2000) 8871–8878. <https://doi.org/10.1021/la000257a>.
- [64] G. Decher, J.D. Hong, J. Schmitt, Buildup of ultrathin multilayer films by a self-assembly process: III. Consecutively alternating adsorption of anionic and cationic polyelectrolytes on charged surfaces, *Thin Solid Films.* 210–211 (1992) 831–835. [https://doi.org/10.1016/0040-6090\(92\)90417-A](https://doi.org/10.1016/0040-6090(92)90417-A).
- [65] Z. Sui, D. Salloum, J.B. Schlenoff, Effect of Molecular Weight on the Construction of Polyelectrolyte Multilayers: Stripping versus Sticking, *Langmuir.* 19 (2003) 2491–2495. <https://doi.org/10.1021/la026531d>.
- [66] C.C. Buron, C. Filiâtre, F. Membrey, C. Bainier, L. Buisson, D. Charrat, A. Foissy, Surface morphology and thickness of a multilayer film composed of strong and weak polyelectrolytes: Effect of the number of adsorbed layers, concentration and type of

- salts, *Thin Solid Films*. 517 (2009) 2611–2617. <https://doi.org/10.1016/j.tsf.2008.10.036>.
- [67] H. Deligöz, B. Tieke, QCM-D study of layer-by-layer assembly of polyelectrolyte blend films and their drug loading-release behavior, *Colloids Surf. Physicochem. Eng. Asp.* 441 (2014) 725–736. <https://doi.org/10.1016/j.colsurfa.2013.10.033>.
- [68] M. Elzbiaciak, M. Kolasińska, S. Zapotoczny, R. Krastev, M. Nowakowska, P. Warszyński, Nonlinear growth of multilayer films formed from weak polyelectrolytes, *Colloids Surf. Physicochem. Eng. Asp.* 343 (2009) 89–95. <https://doi.org/10.1016/j.colsurfa.2009.01.034>.
- [69] C.J. Lefaux, J.A. Zimberlin, A.V. Dobrynin, P.T. Mather, Polyelectrolyte spin assembly: Influence of ionic strength on the growth of multilayered thin films, *J. Polym. Sci. Part B Polym. Phys.* 42 (2004) 3654–3666. <https://doi.org/10.1002/polb.20209>.
- [70] M. An, J.-D. Hong, Surface modification of hafnia with polyelectrolytes based on the spin-coating electrostatic self-assembly method, *Colloids Surf. Physicochem. Eng. Asp.* 348 (2009) 301–304. <https://doi.org/10.1016/j.colsurfa.2009.07.009>.
- [71] G. Liu, J. Zhao, Q. Sun, G. Zhang, Role of Chain Interpenetration in Layer-by-Layer Deposition of Polyelectrolytes, *J. Phys. Chem. B.* 112 (2008) 3333–3338. <https://doi.org/10.1021/jp710600f>.
- [72] M. Elzbiaciak, S. Zapotoczny, P. Nowak, R. Krastev, M. Nowakowska, P. Warszyński, Influence of pH on the Structure of Multilayer Films Composed of Strong and Weak Polyelectrolytes, *Langmuir*. 25 (2009) 3255–3259. <https://doi.org/10.1021/la803988k>.
- [73] J.J. Harris, M.L. Bruening, Electrochemical and in Situ Ellipsometric Investigation of the Permeability and Stability of Layered Polyelectrolyte Films, *Langmuir*. 16 (2000) 2006–2013. <https://doi.org/10.1021/la990620h>.
- [74] R.A. Ghostine, J.B. Schlenoff, Ion Diffusion Coefficients Through Polyelectrolyte Multilayers: Temperature and Charge Dependence, *Langmuir*. 27 (2011) 8241–8247. <https://doi.org/10.1021/la2015258>.
- [75] M. Chirea, V. Garc?a-Morales, J.A. Manzanares, C. Pereira, R. Gulaboski, F. Silva, Electrochemical Characterization of Polyelectrolyte/Gold Nanoparticle Multilayers Self-Assembled on Gold Electrodes, *J. Phys. Chem. B.* 109 (2005) 21808–21817. <https://doi.org/10.1021/jp0537815>.
- [76] F. Caruso, H. Lichtenfeld, M. Giersig, H. Möhwald, Electrostatic Self-Assembly of Silica Nanoparticle–Polyelectrolyte Multilayers on Polystyrene Latex Particles, *J. Am. Chem. Soc.* 120 (1998) 8523–8524. <https://doi.org/10.1021/ja9815024>.
- [77] Z. Zhao, R. Yan, J. Wang, H. Wu, Y. Wang, A. Chen, S. Shao, Y.-Q. Li, A bacteria-activated photodynamic nanosystem based on polyelectrolyte-coated silica nanoparticles, *J. Mater. Chem. B.* 5 (2017) 3572–3579. <https://doi.org/10.1039/C7TB00199A>.
- [78] M. Mathelié-Guinlet, T. Cohen-Bouhacina, I. Gammoudi, A. Martin, L. Béven, M.-H. Delville, C. Grauby-Heywang, Silica nanoparticles-assisted electrochemical biosensor for the rapid, sensitive and specific detection of *Escherichia coli*, *Sens. Actuators B Chem.* 292 (2019) 314–320. <https://doi.org/10.1016/j.snb.2019.03.144>.
- [79] P.D. Howes, R. Chandrawati, M.M. Stevens, Colloidal nanoparticles as advanced biological sensors, *Science*. 346 (2014). <https://doi.org/10.1126/science.1247390>.

Figures legends

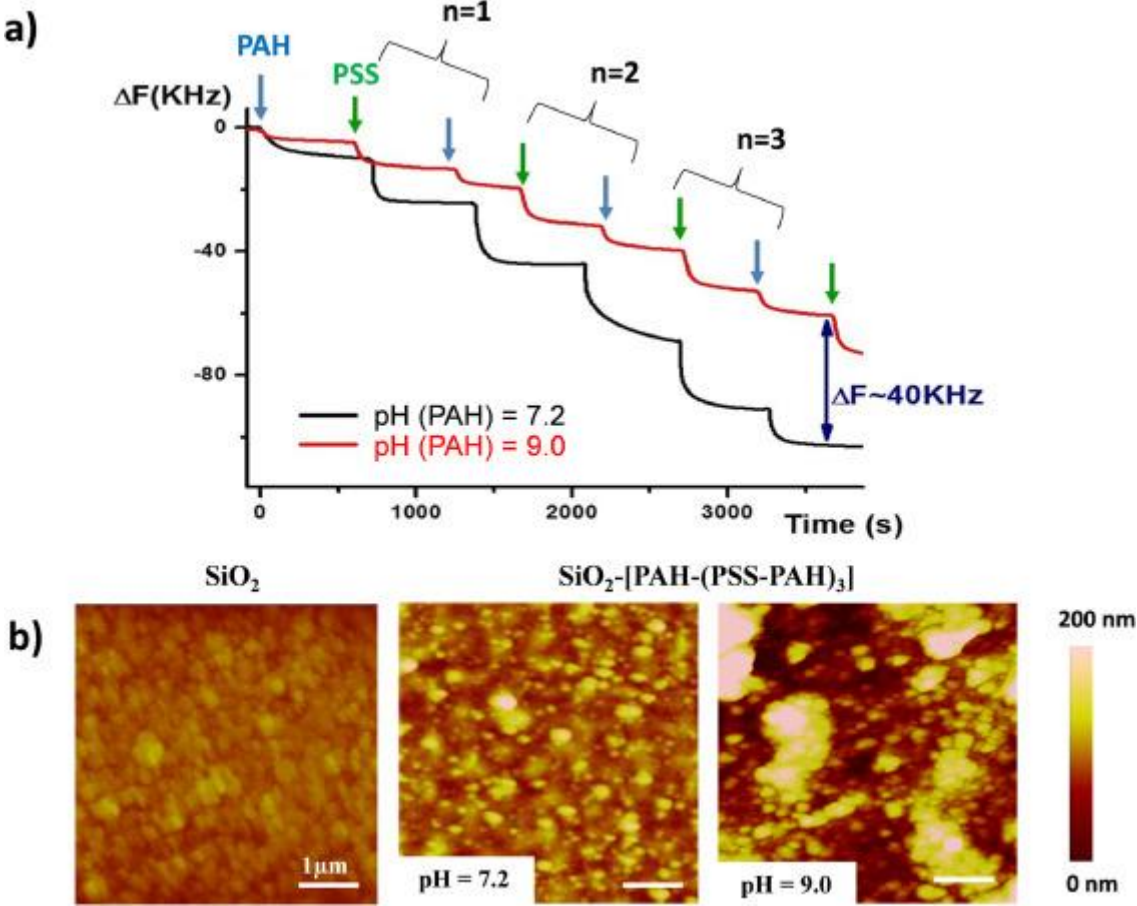


**Figure 1.** a) Real-time evolution of the  $\Delta F_{\text{Love}}$  frequency shifts, measured by Love wave sensors, induced by the sequential deposition of PAH (solution at pH 7.2 or 9.0) and PSS (pH at 7.2). b) AFM height images of bare  $\text{SiO}_2$  surface and  $[\text{PAH}-(\text{PSS}-\text{PAH})_3]$  PEMs at the two studied pH for PAH solutions.

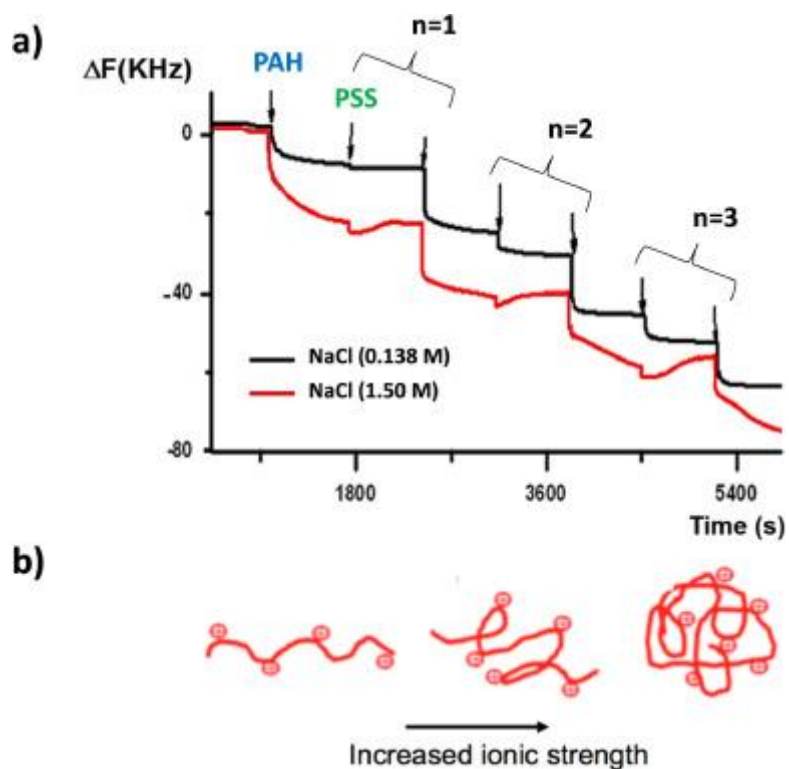


**Figure 2.** a) Real-time variation of the  $\Delta F_{\text{Love}}$  frequency shift, measured by Love wave sensors, induced by the sequential deposition of [PAH-(PSS-PAH)<sub>n</sub>] PEMs (both solutions at pH 7.2) with two different concentrations of NaCl. b) Scheme illustrating the PE conformational changes with an increasing ionic strength.

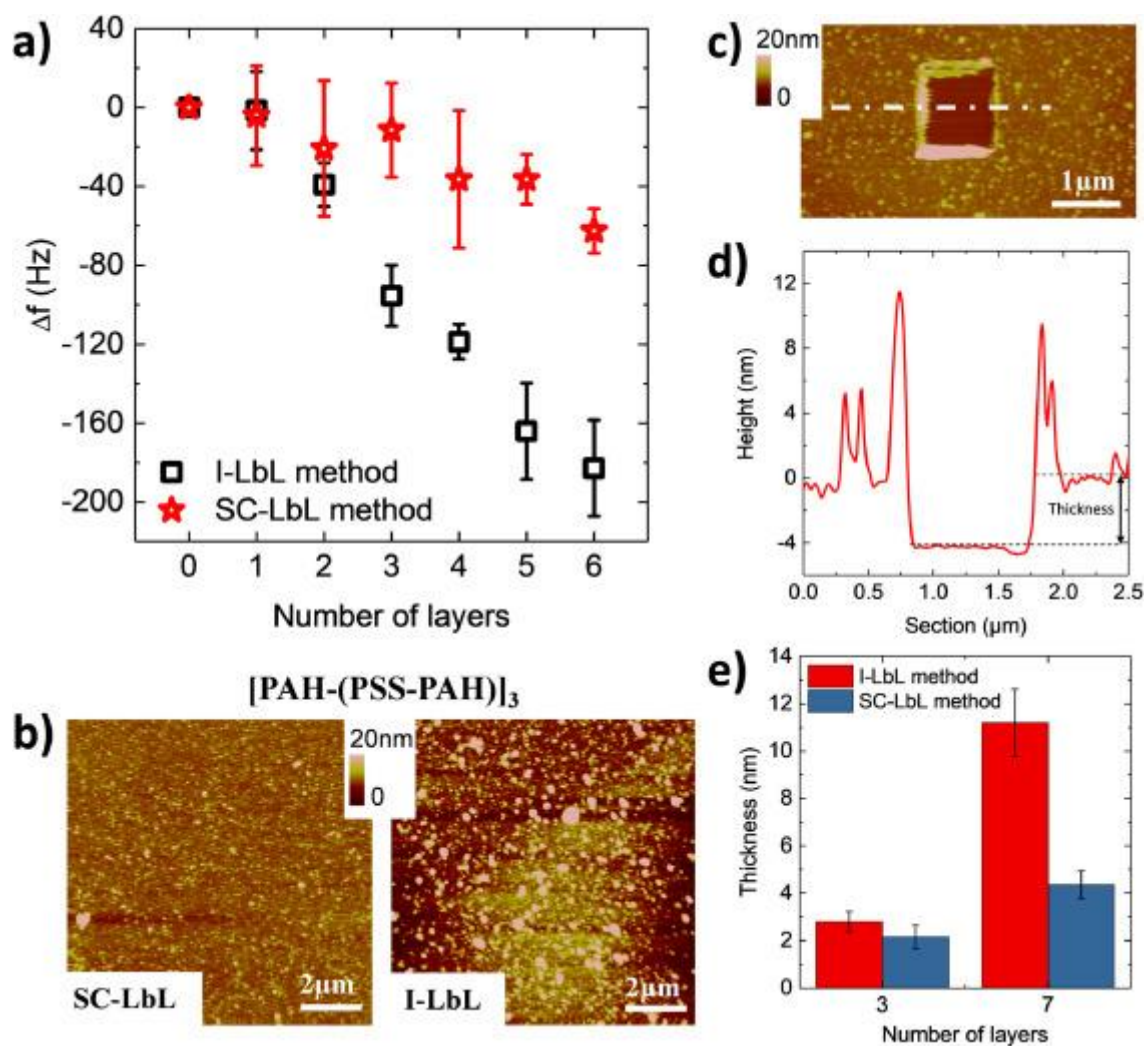


**Figure 3.** Influence of the deposition method on the buildup of [(PSS-PAH)<sub>n</sub>] PEMs on a first layer of PAH deposited on the gold-coated quartz crystal. a) Variation of the  $\Delta f_{\text{QCM}}$  frequency shift in QCM-D experiments, resulting from the sequential deposition of each layer for both I-LbL and SC-LbL methods. b) AFM height images of [PAH-(PSS-PAH)<sub>n</sub>] PEMs built from both methods, performed after drying at ambient temperature. c) AFM height image resulting from a scratching experiment on [PAH-(PSS-PAH)<sub>n</sub>]. d) Height profile along the dotted white line (c) allowing for the determination of the PEM thickness – Because of PEM aggregates and accumulated materials close to the scratched area, higher areas are observed. e) Thickness of PEMs as a function of the number of layers for both I-LbL and SC-LbL methods. Error bars were calculated from three independent experiments.

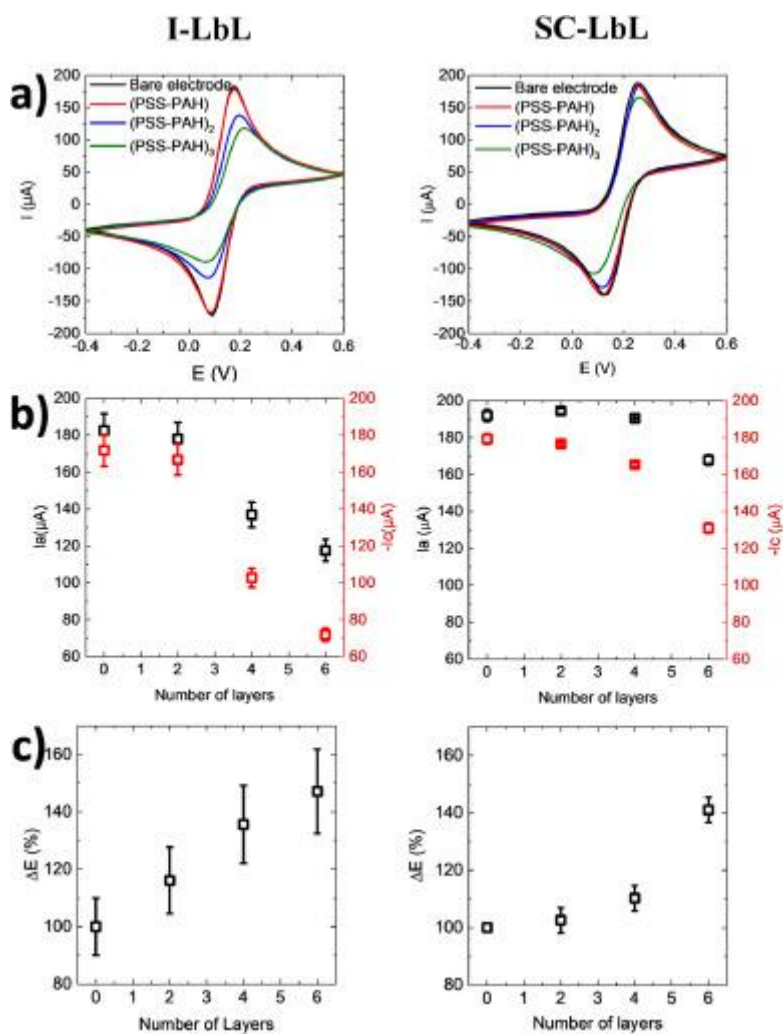


**Figure 4.** Influence of the presence of [(PSS-PAH)<sub>n</sub>] PEMs (n=0, 1, 2, 3) made by the I-LbL and SC-LbL methods, after the deposition of a first PAH layer, on the (a) CV curves, (b) intensities of the oxidation ( $I_a$ ) and reduction ( $I_c$ ) peaks and (c)  $\Delta E=(E_a - E_c)$  peak-to-peak separation, normalized by values obtained on the bare electrode. Error bars were calculated from three independent experiments.

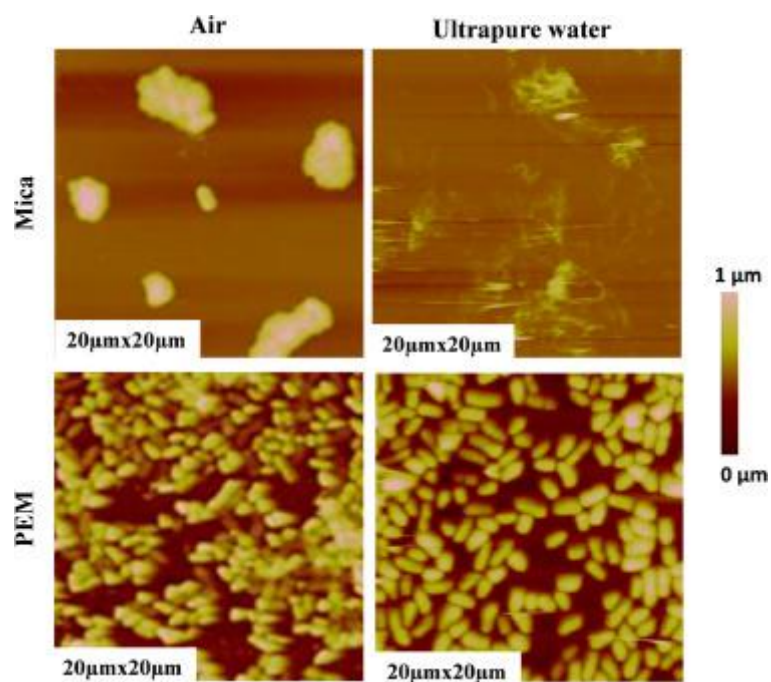


**Figure 5.** AFM height images of *E. coli* bacteria deposited either on a bare mica substrate or on a [PAH-(PSS-PAH)<sub>3</sub>] PEM, and imaged either in air or in ultrapure water.

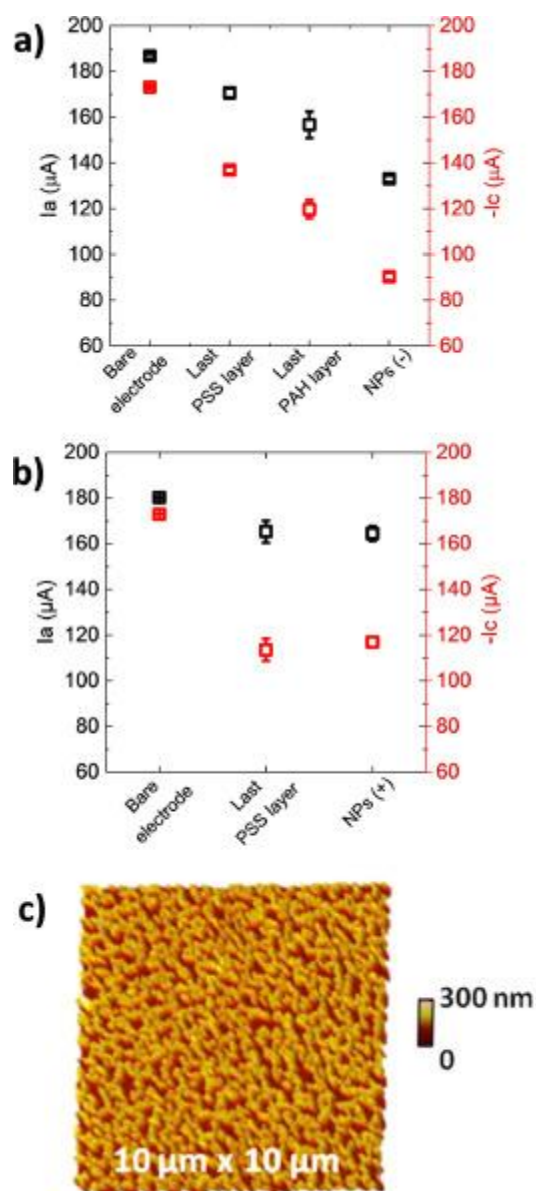


**Figure 6.** Influence on the peak intensities determined from CV curves of the deposited layers: a) [PAH-(PSS-PAH)<sub>3</sub>] PEMs coated with negatively charged NPs, b) [PAH-(PSS-PAH)<sub>3</sub>-PSS] PEMs coated with positively charged NPs. Error bars are calculated from three independent experiments. c) AFM height image of SiO<sub>2</sub>-NP<sup>+</sup> (diameter of 100 nm) covering a [PAH-(PSS-PAH)<sub>3</sub>-PSS] PEM confirming the actual attachment of such NPs during electrochemical measurements.